AIP | Journal of Applied Physics

Magnetic properties and magnetocaloric effect of La0.8Ca0.2MnO3 nanoparticles tuned by particle size

Shaobo Xi, Wenjian Lu, and Yuping Sun

Citation: J. Appl. Phys. **111**, 063922 (2012); doi: 10.1063/1.3699037
View online: http://dx.doi.org/10.1063/1.3699037
View Table of Contents: http://jap.aip.org/resource/1/JAPIAU/v111/i6
Published by the American Institute of Physics.

Magnetic properties and magnetocaloric effect of $La_{0.8}Ca_{0.2}MnO_3$ nanoparticles tuned by particle size

Shaobo Xi,[1,2] Wenjian Lu,[3,a)] and Yuping Sun[1,3]
[1]*High Magnetic Field Laboratory, Chinese Academy of Sciences, Hefei 230031, China*
[2]*Department of Physics, University of Science and Technology of China, Hefei 230026, China*
[3]*Key Laboratory of Materials Physics, Institute of Solid State Physics, Chinese Academy of Sciences, Hefei 230031, China*

(Received 12 December 2011; accepted 26 February 2012; published online 30 March 2012)

$La_{0.8}Ca_{0.2}MnO_3$ particles with the sizes from 17 to 43 nm have been prepared using the sol-gel method and the magnetic properties are systematically studied. The existence of the blocking of the superparamagnetism (SPM), freezing of super-spin-glass, and surface-spin-glass is evidenced. It is found that a core-shell structure can be responsible for the magnetism behavior of the nanoparticles. The phase transition from paramagnetism (PM) to ferromagnetism (FM) is modified from first order to second order as the particle size reduced. The magnetocaloric effect (MCE) thus is modified by the changed magnetism. The observed temperature interval of the magnetic entropy change broadens as the particle size reduced. The magnetic entropy change of superparamagnetic particles has been calculated based on the core-shell model. The relative cooling power (RCP) can be tuned dramatically by particle size due to the change of spontaneous magnetization of the core and the changed ratio of the shell and surface, which shows different behavior in magnetization.
 [http://dx.doi.org/10.1063/1.3699037]

I. INTRODUCTION

In the past few decades, mixed valence manganites have been investigated experimentally and theoretically due to the interesting and rich electronic and magnetic properties.[1,2] The colossal magnetoresistance (CMR) is closely related to the ferromagnetic-paramagnetic (FM-PM) phase transition. The nature of the magnetic phase transition in manganites and the relationship with their physical properties are still unclear. For example, in the optimally doped compound $La_{2/3}A_{1/3}MnO_3$ (A = alkaline earth ion) it has been found that the FM-PM phase transition is of first order for Ca,[3,4] but of second order for Sr.[5]

Beyond the CMR some manganite systems exhibit also a relatively strong magnetocaloric effect (MCE) around the first order FM-PM transition temperature. Magnetic refrigeration, based on MCE, has received increasing attention as an alternative to the well-established compression-evaporation cycle for room-temperature applications since it is higher in cooling efficiency, environmentally friendly and can be more compactly build as the solid substances are the working materials.[6,7] Several alloy materials have been found to exhibit large MCEs, such as $La(Fe_{1-x}Si_x)_{13}$, $MnFeP_xAs_{1-x}$, and $Ni_{2-x}Mn_{1-x}Ga$ Heusler alloys. However there are several disadvantages in these promising materials, such as large thermal and/or field hysteresis and expensive production cost, which are not beneficial for the actual magnetic refrigerant application.[8,9] Manganites with small thermal and magnetic hysteresis and relatively low cost make them a promising material for refrigeration since the large MCE was found in $La_{0.8}Ca_{0.2}MnO_3$ single crystal.[10] Another advantage of their potential applications is the broad working temperature ranges due to easy controlling of the Curie temperature by doping routes. The disadvantage of the first-order transition of manganites is the sharp FM-PM phase transition that induces a narrow interval of the magnetic entropy change and hence small relative cooling power (RCP), while recent researches reported that the MCE can been tuned by the grain size. With a decrease in the grain size of $La_xCa_{1-x}MnO_3$ particles to a few ten nanometers, the FM-PM phase transition has changed into second order and the MCE has also been greatly changed.[11–13] Thus it is significant to study the size effect on MCE. It is still not quite clear about the physical origin of the change of magnetic properties with the grain size.[14] Hueso *et al.* assumed that this property is due to the differences between core and surface,[11] but the details of the transition as well as how it acts on MCE are under debate.

As reported by some authors, nanoscaled magnetic particles usually exhibit a number of outstanding physical properties such as superparamagnetism (SPM), super-spin-glass, and surface-spin-glass behaviors.[15–17] The particles become single domain as the size reduced to a value smaller than the critical radius r_c.[18] In an isolated noninteracting single domain particle ensemble it shows a SPM behavior since each particle can be considered as a large magnetic dipole, which behaves like a paramagnetic atom, proposed by Néel[19] and Brown.[20] If the magnetic dipole interaction between particles are strong enough the super-spin-glass dominates the magnetism of the nanoparticles.[17,21,22] On the other hand as the particle size decreased the number of surface atoms can be comparable with inner atoms, thus the magnetic behavior is mainly dominated by spin disordered nonmagnetic surface. Lowered saturate magnetization and enhanced surface-spin-glass can be observed in a various small particle systems.[23,24]

In this study, we present a systematic investigation of magnetic characteristics of $La_{0.8}Ca_{0.2}MnO_3$ manganite associated with the finite-size effects, and evidenced SPM,

a)Corresponding author. Email: wjlu@issp.ac.cn.

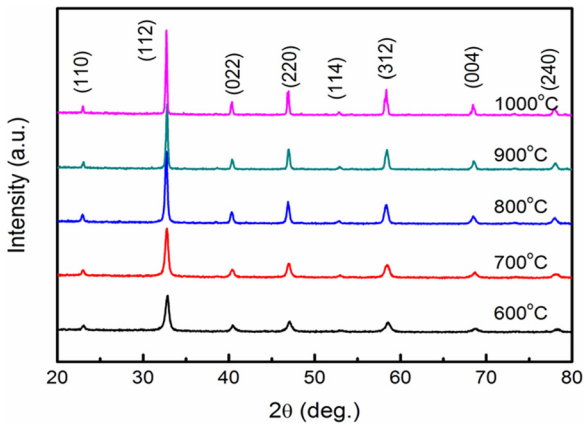

FIG. 1. X-ray diffraction patterns of the samples annealed at various temperatures.

super-spin-glass, and surface-spin-glass existing in the nanoparticle sample. The FM-PM phase transition was found to change from first order to second order as particle size decreases. The cause of this change was investigated and a core-shell model was suggested to explain the magnetic characteristics of nanoparticles. Tuning of the magnetocaloric property thus can be obtained through modifying the size of the particles and this tuning is likely to be applicable for other magnetocaloric materials.

II. EXPERIMENTAL DETAILS

Analytical grade La_2O_3 and $CaCO_3$ weighed accurately were dissolved in nitric acid and mixed with $Mn(NO_3)_2$ solution in de-ionized water to obtain a clear solution with mole ratio of La:Ca:Mn = 0.8:0.2:1. Citric acid ($HOOCCH_2C(OH)(COOH)CH_2COOH$) with a molar ratio of citric acid/total metal ions being 1.2 were weighed, and added to the mixed solution. Ammonia was used to adjust the ph value to 7. A suitable amount of polyethylene glycol was added to the solution and stirred vigorously obtaining a transparent viscous solution. After achieving complete dissolution, the resultant solution was heated at 110 °C for 8 h in order to evaporate the excess solvents and promote polymerization. The solution became highly viscous, with a change from yellow to orange, and finally it is gelled to a glassy resin. The gel was further heated in a box furnace at 250 °C, and brown precursor was obtained. This powder was divided into several parts and annealed at 600 °C, 700 °C, 800 °C, 900 °C, and 1000 °C for 8 h, respectively, and black $La_{0.8}Ca_{0.2}MnO_3$ powders were obtained.

TABLE I. Particle size D of $La_{0.8}Ca_{0.2}MnO_3$ sample annealed at different temperatures T_{anneal}.

T_{anneal} (°C)	600	700	800	900	1000
D (nm)	17.0	19.5	28.0	35.5	43.0

The X-ray diffraction (XRD) with Cu-$K\alpha$ radiation (Philips X'pertPro) was used to determine the crystal structure, lattice parameters, and crystallite sizes. XRD patterns were analyzed by the Rietveld method. The magnetization measurements were carried out by using a Quantum Design superconducting quantum interference device (SQUID) in the temperature range of 5–380 K. The surface morphology of samples was studied by field-emission scanning electronic microscopy (FE-SEM).

III. RESULTS AND DISCUSSIONS

The XRD patterns of nanocrystalline $La_{0.8}Ca_{0.2}MnO_3$ particles were shown in Fig. 1. The diffraction peaks can be indexed in the orthorhombic setting of the *Pnma* space group. The average crystallite sizes D calculated by using the Debye-Scherer equation were shown in Table I. The SEM graph in Fig. 2 confirmed the calculated size generally. For the sample annealed at 600 °C the size observed on SEM graph is larger than that derived by XRD pattern mainly due to the aggregation of small particles.

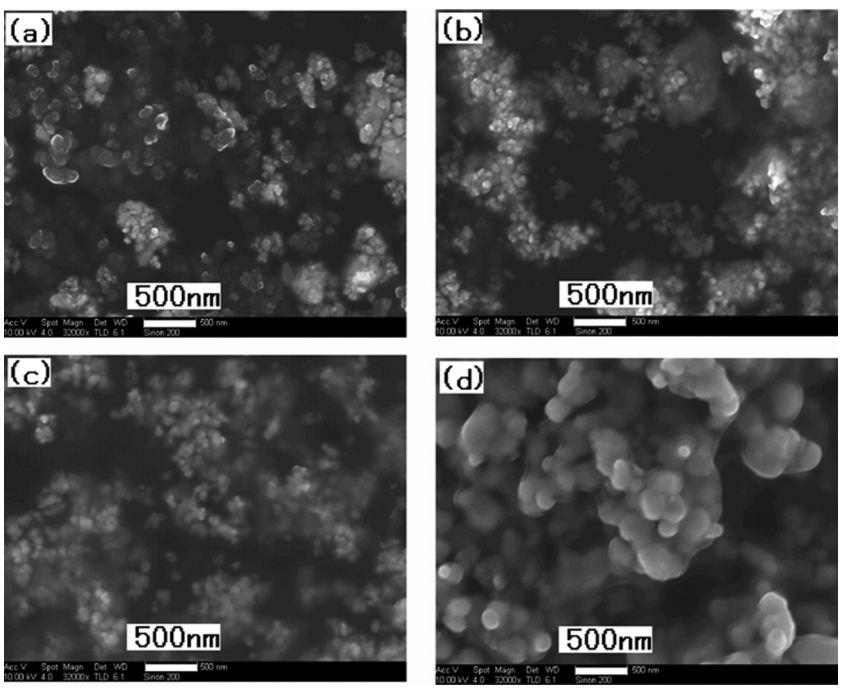

FIG. 2. SEM micrograph of samples annealed at various temperatures of (a) 600 °C, (b) 700 °C, (c) 800 °C, and (d) 1000 °C.

Figure 3 presents the temperature dependence of the dc magnetization via zero-field-cooled (ZFC) and field-cooled (FC) processes with an applied field of 0.01 T. The *M-T* data suggests that all these samples undergo a PM to FM transition upon cooling. The critical temperatures T_C are 234, 252, 214, 237, and 236 K for 17, 19.5, 28, 35.5, and 43 nm samples respectively. The T_C is defined as the valley of dM/dT in the M (T) curves. The ZFC magnetization at low temperatures shows a gradual increase in the relatively small particle. The ZFC magnetizations of the 17, 19.5, and 28 nm samples in Fig. 3 exhibit a maximum at 83 K, 76 K, and147 K, respectively, while the ZFC and FC curves begin to diverge at 218, 244, and 253 K well above the temperature corresponding to the maximum magnetization. Both of the two characteristics may indicate the SPM existing in these samples. In the *M-T* curves the temperature corresponding to the maximum magnetization (T_p) is defined as blocking temperature T_b and the temperature where the ZFC and FC curves begin to diverge is defined as irreversible temperature T_{irr}. Moreover from the FC curves of the 17, 19.5, and 28 nm samples, plateaus can be seen as the temperatures are lowered mainly indicating the freezing of spin-glasses state.

To confirm the SPM or the spin-glass of the samples, we have investigated the H dependence of T_p by measuring the temperature dependence of ZFC magnetization of the 17 nm samples recorded for wide range of applied magnetic fields as shown in Fig. 4. Thus dependence of T_p on H can be derived as shown in Fig. 5. The enlarged plots of T_p-H curve at low and high fields are shown in the insets of Figs. 5(a) and 5(b), respectively. The figures show that T_p shifts with H following three types of patterns. T_p decreases very quickly with increasing applied field for $H \leq 0.05$ T and decreases slowly with further increasing field for 0.05 T $\leq H \leq$ 0.1 T. For $H \geq 0.2$ T it decreases very slowly compared with that at low fields. These three types of T_p may arise from the different magnetic states dominating under different applied fields as discussed below.

The glassy or SPM system in the mean-field approximation can survive in the presence of certain magnetic fields below so called Almeida-Thouless (AT) line in *H-T* phase

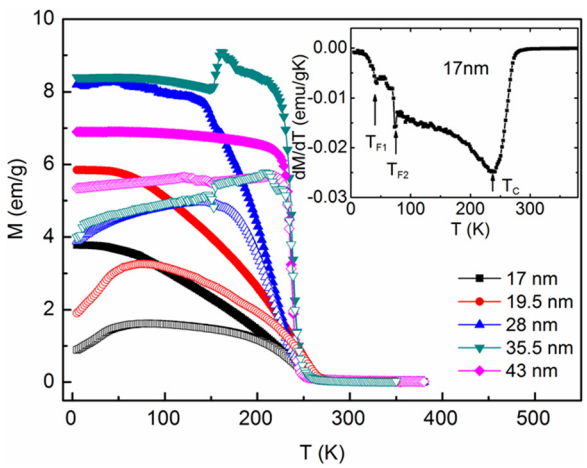

FIG. 3. Temperature dependence of magnetization recorded in the ZFC (open symbols) and FC (solid symbols) modes under an applied magnetic field $H = 0.01$ T. Inset shows the first derivative of *M-T* curve in FC model for the 17 nm sample.

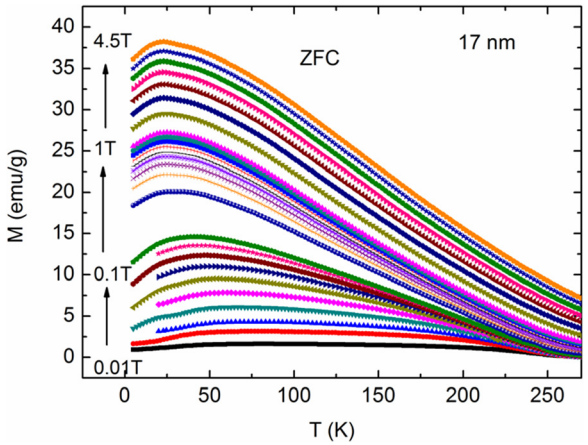

FIG. 4. Temperature dependence of ZFC magnetization of the 17 nm sample in different applied magnetic fields.

diagram.[25,26] AT-line in this case corresponds to the phase boundary between SPM and spin-glass like phases and can be written as

$$T_p = T_f[1 - (H/H_a)^{\alpha}], \quad (1)$$

where T_f is freezing temperature at $H = 0$ for glassy system, and for SPM T_f denote T_b at $H = 0$; $H_a = 2K_{eff}/\rho M_s$ presents the critical field below which the SPM or the spin-glass phase can survive, and above which the SPM phase or spin-glass phase disappears since at this critical field the T_p was suppressed to 0 K. K_{eff} is effective anisotropy constant, M_s saturation magnetization, and ρ density of the sample. Parameter α depends on the interaction strength. For SPM $\alpha = 2$,[27] while for super-spin-glass and surface-spin-glass this parameter is close to 2/3.[28,29]

By fitting this expression to the experimentally obtained data, good agreements are achieved for the 17 nm sample with different parameters as shown in the insets of Figs. 5(c) and 5(d): $\alpha = 2$, $H_a = 0.096$ T, and $T_f = 83.4$ K under the applied field of $H \leq 0.05$ T; $\alpha = 2/3$, $H_a = 0.29$ T, and

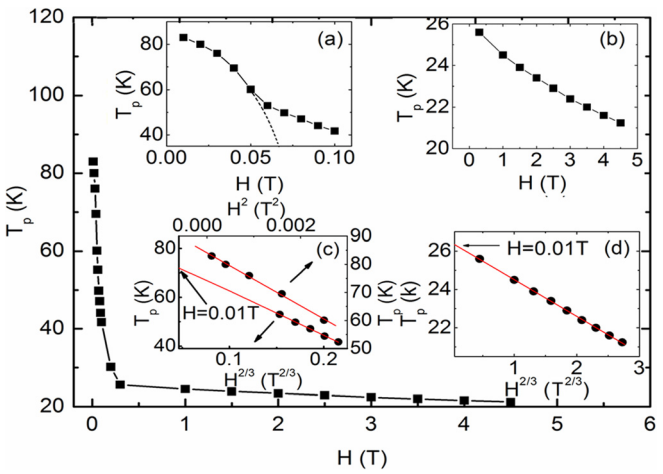

FIG. 5. H dependence of T_p (solid line to guide the eye). Inset: (a) T_p vs H for $H \leq 0.1$ T; Dashed curve is the fitting SPM curve extrapolated to the field higher than 0.05 T. (b) T_p vs H for 0.2 T $\leq H \leq$ 4.5 T. (c)-(d) Fitting AT line to the experimentally obtained data (circle points). A good agreement was achieved by using parameters: $\alpha = 2$ for $H \leq 0.05$ T $\alpha = 2/3$ for 0.06 T $\leq H \leq$ 0.1 T, and $\alpha = 2/3$ for 0.2 T $\leq H \leq$ 4.5 T.

$T_f = 81.0$ K under the field of 0.06 T $\leq H \leq$ 0.1 T; $\alpha = 2/3$, $T_f = 26.5$ K, and $H_a = 48.8$ T under the field of $H \geq 0.2$ T. The obtained fitting value $\alpha = 2$ indicates the presence of SPM at the applied field lower than 0.05 T and $\alpha = 2/3$ indicates the super-spin-glass or surface-spin-glass phase existing in this sample, which always present in the nanoparticle samples. Since for both super-spin-glass and surface-spin-glass phases, $\alpha = 2/3$, it is difficult to distinguish whether or not the system behaves as a super-spin-glass or surface-spin-glass. Nevertheless, in super-spin-glass system, the low temperature spin-glass phase is very sensitive to the magnetic field and the application of a low field can make it disappear.[25,30] While for surface-spin-glass-sample, the spin-glass phases can survive at a very high field[29,31] due to the large K_{eff} induced by the surface anisotropy. In our sample we can see that for 0.06 T $\leq H \leq$ 0.1 T, the obtained fitting value of $H_a = 0.29$ T, that is to say the spin-glass phase can survive only at a field lower than 0.29 T, which indicates the super-spin-glass dominates the shifting of T_p under an applied field of 0.06 T $\leq H \leq$ 0.1 T. While for the case of $H \geq 0.2$ T, $H_a = 48.8$ T. That is to say the spin-glass phase can remain at a very high field, indicating the surface-spin-glass presents under an applied filed of $H \geq 0.2$ T. Thus the coexistence of SPM, super-spin-glass- and surface-spin-glass was identified by the AT line fitting. the T_f of surface-spin-glass and super-spin-glass is defined as T_{f1} and T_{f2}, respectively.

It can be seen from the fitting data that all of the three fitting H_a are higher than a certain low field, which means that all these phases can survive at a low field. On the other hand we can see from the fitting values that $T_{f1} < T_{f2} < T_b$, thus we can deduce that the sample undergoes surface-spin-glass, super-spin-glass, blocked SPM, SPM, and PM state, respectively from the low temperatures to the high temperatures under a ZFC warming procedure at a low applied field (0.01 T, for example). However actually there is only SPM-induced T_b at 83 K can obviously be seen at the ZFC procedure at an applied field of 0.01 T. It seems that no evidence of surface-spin-glass and super-spin-glass can be seen in the ZFC curve. But we can see two sudden increases of the magnetization at 43 K and 75 K, respectively from the FC curve. We can more clearly find such two sudden increases by the observation of two valleys existing in the dM/dT curve at $T_{F1} = 43$ K and $T_{F2} = 75$ K, respectively (see the inset in Fig. 3). The sudden increase in FC curve is induced by the onset of freeing of spin-glass state, which is a little higher than the spin-glass freeing temperature T_f.[28] As we extrapolate the fitted data to 0.01 T for the super-spin-glass line and surface-spin-glass line shown in Figs. 5(c) and 5(d), the freezing temperatures of surface-spin-glass and super-spin-glass are 26.2 K and 71.5 K, respectively. We can see that $T_{F1} = 43$ K is a little higher than the super-spin-glass freezing temperature of 26.2 K. Therefore T_{F1} could be considered as the temperature of onset of freeing of the surface-spin-spin-glass. Moreover it can be seen from the FC curve of 17 nm sample in Fig. 3 that the M (T) curve becomes a plain plateau below 26 K indicating the complete freezing of the surface-spin is achieved at this temperature, which is perfectly consistent with the extrapolating derived freezing temperature of 26.2 K. Similarly $T_{F2} = 75$ K is a little higher than the value of $T_{f2} = 71.5$ K derived from fitting super-spin-glass line. So we may conclude that T_{F2} is the temperature at which the freezing of super-spin-glass begins to emerge. The fitting values of T_{f1} and T_{f2} are perfectly consistent with the T_{F1} and T_{F2} confirms our fitting is correct. Therefore the super-spin-glass and surface-spin-glass indeed coexist in our sample.

Since there are SPM, super-spin-glass, and surface-spin-glass existing in the 17 nm sample, a core-shell structure in our sample can be considered: The core is a single domain ferromagnetic particle with SPM or super-spin-glass behavior at certain temperature while the shell is spin-disordered surface layer with the surface-spin-glass behavior at low temperatures (below 26.5 K according to the fitting parameter T_f). Moreover because the surface-spin-glass and SPM/super-spin-glass exist at the surface shell and inner core, respectively, the magnetization of the surface-spin-glass will be superimposed on that of the SPM/super-spin-glass in inner cores. That is to say the surface behavior is independent with the inner core behavior. On the other hand in the inner core the SPM and super-spin-glass also exist independently. The evidence is the sudden increase in FC curve at 75 K at 0.01 T, which is well consistent with the T_p derived from the dependently fitting data of super-spin-glass.

As discussed above the SPM-induced peaks dominate the magnetization maximum in ZFC curves at a low applied field. With the increasing field the SPM-induced peak shifts to 0 K at $H = 0.096$ T (that is to say the blocked SPM is suppressed by increasing field and should disappear above field larger than H_a). But actually starting from 0.06 T the shifting of the peak does not follow the SPM model but follow the super-spin-glass model instead. Assuming the SPM model is followed at fields larger than 0.06 T the peak should follow the dashed curve which lies below the super-spin-glass induced peak as shown in inset of Fig. 5(a). It seems that the SPM-induced peaks are smeared by the super-spin-glass induced peak since the later lies at higher temperature. When at the even higher field (larger than 0.29 T) the super-spin-glass was suppressed to 0 K and disappears. Thus the peaks shift following the surface-spin-glass model. Above this field both the blocking of SPM and the freezing of super-spin-glass disappear. In other word for an applied field higher than 0.29 T, the magnetic behavior of our sample is dominated by the magnetization of superparamagnetic core and surface-spin-glass shell. This conclusion is important for discussing the MCE of our samples as will be discussed latter. We also investigated the T_p dependence of H of the 28 nm sample. The result is quite similar to that for 17 nm sample and shows the coexistence of the SPM, super-spin-glass and relatively weak surface-spin-glass.

The SPM and super-spin-glass exist in various magnetic nano-systems, which is usually termed an interacting superparamagnets or interacting nanoparticles assembly.[30–32] When interparticle interactions are negligible the system possesses superparamagnetic behavior where superspins oscillate between their easy directions of magnetization and freeze along these direction below blocking temperature T_b. In the case of sufficiently strong interaction among superspins, usually high degree of their frustration is also present due to the existence of certain distribution of particles size and shape, interparticle distances, etc. The dipole interaction of powder sample has been confirmed and the magnetic

property has been changed evidently compared with dispersed non-interacting samples.[33] This situation causes the creation of the super-spin-glass state below certain freezing temperature T_f. In case where two nanoparticle systems differ only in the strength of interparticle interactions (diluted and concentrated particles), the common situation is that $T_b < T_f$[30] since contribution of interparticle interactions superimposes on the blocking process. While in our 17 nm powder sample $T_b > T_f$ mainly because the distances between particles induce weaker dipole interaction. In our 17 nm sample, the moment in each particle is very large (about 30000 μ_B derived from the spontaneous magnetization of the sample considering the particles as spherical magnetic dipoles. Two magnetic dipoles with moment m_1 and m_2 separated by a distance r have the potential energy[34]

$$E = \frac{\mu_0 m_1 m_2}{4\pi r^3}. \quad (2)$$

If we assume the particles are closely packed, the magnitude of the dipolar potential energy of two moments can be estimated by this equation. In ground state $m = 30000\ \mu_B$, and $r = 17$ nm, It turns out to be $E = 2.5 \times 10^{-21}$ J, which is equivalent to about 183 K in temperature. According to the reports of Markovich *et al.* the 18 nm $La_{0.8}Ca_{0.2}MnO_3$ sample, which was compacted under pressure into cylinder samples with the density about 60% of the density of the bulk crystal, has the T_f about 188 ± 31 K,[35] which approaches the calculated potential energy of 183 K. In our 17 nm sample, the $T_{f=}$ 81 K, which is much smaller than the compacted 18 nm sample and the calculated potential energy. This may be due to the weakened dipole interaction induced by the interspaces between particles in powder sample.

Considering the Mn^{3+}-Mn^{4+} double-exchange mechanism is mainly responsible for the magnetism and conduction of the doped magnetite $La_{0.8}Ca_{0.2}MnO_3$, the origin of the surface-spin-glass layers formation in the nanoparticles may be due to the existence of broken bounds at the surface and the translational symmetry breaking of the lattice, generating randomness in the double exchange interactions.[36] The Mn environment at the surface is not the same as that inside the grains, inducing disordered spins at the grain surface. In other words, a core-shell type structure can be proposed:[37] the core is metallic and FM while the shell is insulating and spins are disordered. Although it is difficult to directly assert that disorder is confined in a well delimited surface layer or a progressive disorder process from the inner part of the particles to the surface, the core-shell structure model is suitable for the $La_{0.8}Ca_{0.2}MnO_3$ nanoparticles. The existence of a distorted structure at the surface of the magnetite nanoparticles has also been indirectly supported by the observation of surface phonon,[38] which was seen from the oxygen isotope infrared spectra for $La_{2/3}Ca_{1/3}MnO_3$ samples with small grain size.

As seen in Fig. 3 the behavior of the 19.5 nm sample is similar to that of the 17 nm sample except for the enhanced magnetization, which is caused by more core spins. For the 28 nm sample the ZFC magnetization blocked at 158 K much higher than that of the 17 nm samples, which is due to their volume of a single domain particle containing larger magnetic movement in the 28 nm sample. As discussed above, the samples with small particles (17, 19.5, and 28 nm) are of single domain. The magnetic behavior of the core is dominated by SPM and the super-spin-glass while the surface behavior was dominated by surface-spin-glass. Therefore the slop of transition is not as steep as the bulk counterpart as shown in Fig. 3.

On the other hand the magnetization of the 35.5 and 43 nm samples show very sharp transition, which is much similar to the case of the bulk sample. It indicates that both of the two samples are no longer single domain but multi-domain. Meanwhile the surface spin can be ignored compared to the core spin; therefore the surface effect cannot be observed in both the samples.

Isothermal *M-H* curves of the 17, 28, and 43 nm samples were measured in the applied fields up to 4.5 T at small temperature intervals and the results are shown in Fig. 6. The magnetization of the 43 nm sample saturates at high field and behaves like the bulk materials, but for the 17 nm and 28 nm samples the magnetizations do not saturate. According to core-shell structure the magnetizations of 17 nm and 28 nm samples can be expressed as $M(H) = M_{core} + M_{shell}$, where M_{core} is the superparamagnetic magnetization that saturates at field less than 1 T following a Langevin-like function $M_{core} = N\mu_s L(\alpha)$, where $L(\alpha) = coth(\alpha) - 1/\alpha$, $\alpha = \frac{\mu_s H}{kT}$, μ_s is the magnetic moment of the a single domain particle decided by spontaneous magnetization of the core, which can be derived from the linear extrapolation of *M-H* curve from $H > 1$ T to 0 T , H is the applied field, k is Boltzmann constant, and T the temperature. M_{shell} is magnetic disordered shell component, which is approximately linear after the linear contribution (χH).[39] In Fig. 6(d) we plot M_{core}, versus H (black point) at 220 K after the linear contribution χH was subtracted using Langevin-like function and the curve was shown as solid line. The discrepancy may be due to the size distribution of our sample and the nonlinear $M(H)$ behavior of the shell at low field. According to the above discussion

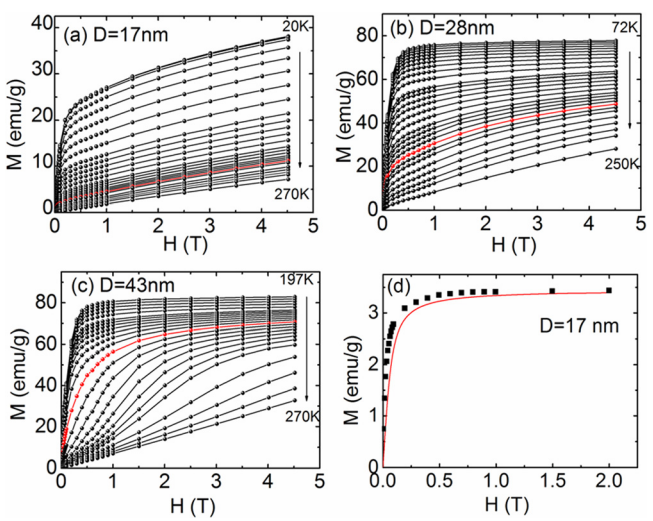

FIG. 6. (a)-(c) Initial magnetization isotherms *M (H)* for the 17, 28, and 43 nm samples at different temperatures around magnetic transition temperature (T_C). The red curve is the data measured at T_C; (d) Magnetization as a function of applied field at $T = 220$ K (solid squares) associated to the Langevin behavior (red curve) of 17 nm sample.

we can conclude that at low field the ferromagnetic core dominates the magnetism, which behaves as SPM. While in high field ($H > 1$ T), the core saturates but the nonmagnetic shell does not saturate inducing the slowly increased magnetization.

As we can see from Fig. 6(c) some of the curves exhibit a kink that is commonly associated with the first-order magnetic phase transitions in the 43 nm sample. While the isotherms of the 17 nm and 28 nm samples in Figs. 6(a) and 6(b) are almost equally spaced and it is difficult to distinguish the critical point.

In order to check the nature of the magnetic transitions, we have used the Banerjee criterion[5,40] to plot the H/M versus M^2 curves in the critical region. The slope of the resulting curves denotes whether a magnetic transition is of first or second order. From a thermodynamic point of view it can be deduced that, if all the curves have a positive slope, the magnetic transition is of second order. On the other hand, if some of the curves show a negative slope at some point, the transition is of first order. For the larger grain-size sample (43 nm sample for example), some of the curves show a negative slope, which is the sign of a first-order magnetic phase transition (see Fig. 7(c)). For the small and intermediate grain-size sample (17 and 28 nm samples), the second-order characters are present (see Figs. 7(a) and 7(b)).

We also investigated the temperature dependence of spontaneous magnetization $M_s$in order to check the phase transition behavior of the inner magnetic core. Figure 7(d) shows the spontaneous magnetization M_s versus temperature for the 17 nm, 28 nm, and 43 nm samples. M_s was derived from the linear extrapolation of M-H curve from $H > 1$ T to 0 T. That is to say the linear term of the shell is subtracted therefore the derived M_s is of the magnetic core. In fact the magnetization of the shell is not exactly linear especially at low field but it can be ignored according to fitting the subtracted value to the Langevin function. We can see that the M_s of the 17 nm sample is much lower than that of the 43 nm sample and increases linearly with decreasing temperature indicating the presence of second order phase transition, while for the 43 nm sample it has an abrupt increase below T_C indicating the presence of first order phase transition. This result shows that the intrinsic magnetization of the sample changed with particle size. In the case of Heisenberg spin clusters, the temperature dependence of magnetization including finite size effects is given by a power law of the form[41]

$$M_s = M_0(1 - BT^{\varepsilon}), \tag{3}$$

where M_0 is the spontaneous magnetization at 0 K, and B is a constant related to the exchange integral, J ($B \propto 1/J^{1/\varepsilon}$). Equation (3) is known as the Bloch $T^{3/2}$ law with $\varepsilon = 3/2$, which has been verified experimentally for most of the bulk magnetic materials. A fitted magnetization data using Eq. (3) is present in Fig. 7(d) (solid lines) with $M_0 = 39.338$ emu/g, $B = 2.00828 \times 10^{-4}$ K^{-1}, and $\varepsilon = 1$ for 17 nm sample. For the 28 nm sample $M_0 = 79.1654$ emu/g, $B = 8.8139 \times 10^{-7}$ K$^{-2.3905}$, and $\varepsilon = 2.3905$. For the 43 nm sample $M_0 = 96.69$ emu/g, $B = 5.08746 \times 10^{-9}$ K$^{-3.25501}$, and $\varepsilon = 3.25501$. The magnetizations therefore do not follow the Bloch's law. For fine particles and clusters some theoretical calculations as well as experimental results[42] have shown rather a wide range of the values of ε between 0.3 and 2.

As a result of this evolution in the magnetic phase transition, some of the properties related to it is also modified in a similar way. One of them is the magnetocaloric effect, that is, the magnetic entropy change (ΔS_M) in the phase transition produced by changes in the magnetic field applied to the

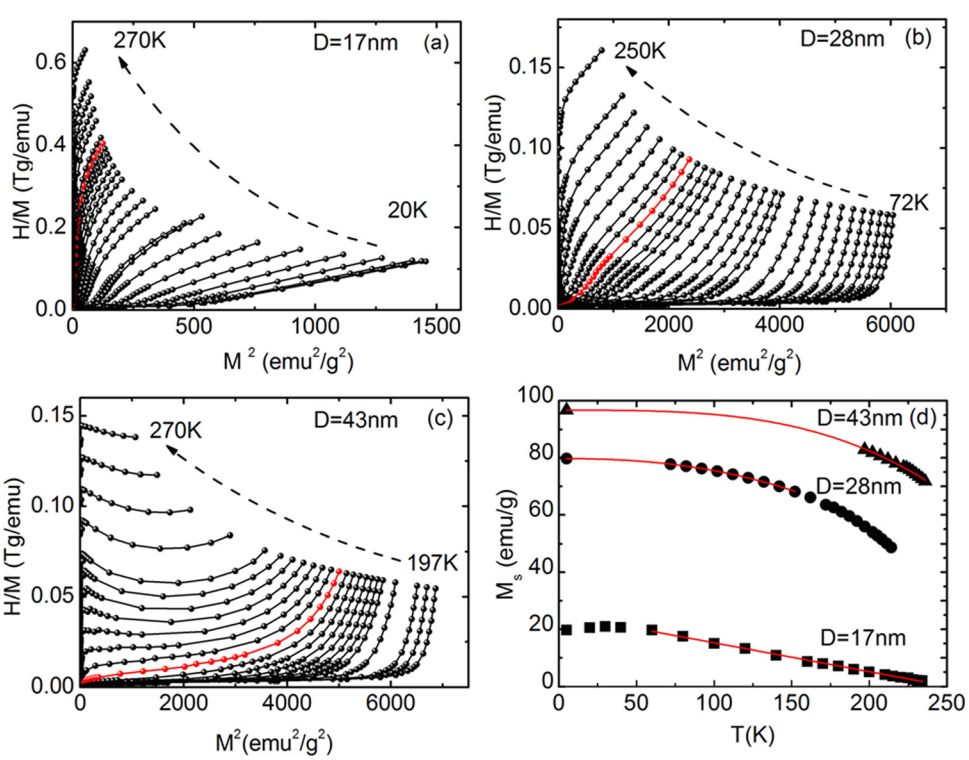

FIG. 7. (a)-(c) Arrott plots (H/M vs M^2) of the 17, 28, and 43 nm samples. The red curve is the data at magnetic transition temperature (T_C); (d) Spontaneous magnetization as a function of temperature for the 17, 28, and 43 nm samples. Solid curve is the fitting data by using the power law form of $M_s = M_0(1 - BT^{\varepsilon})$.

system. The basis of the relationship between magnetic measurements and the change in entropy follows the Maxwell equation[43–45]

$$\left(\frac{\partial S}{\partial H}\right)_T = \left(\frac{\partial M}{\partial T}\right)_H. \quad (4)$$

Integrating and making an approximation suitable for discrete measurements, we obtain

$$\Delta S_M = \Sigma \frac{M_n - M_{n+1}}{T_{n+1} - T_n} \Delta H, \quad (5)$$

where M_n and M_{n+1} are the magnetization values measured in magnetic field H at temperatures T_n and T_{n+1}, respectively. From Eq. (5), ΔS_M associated with the magnetic field and/or temperature variation has been calculated from the measured M (H) curves. The calculated ΔS_M are plotted as a function of temperature with different magnetic field changes of $\Delta H =$ 0.5–4.5 T as shown in Figs. 7(a)–7(c). As expected from Eq. (5), the peak of ΔS_M may occur around T_C where the variation in magnetization as a function of temperature is the sharpest. Obviously, for the 28 nm and 43 nm samples, the peaks of ΔS_M are around T_C, while for the 17 nm sample it locates at a temperature much lower than T_C. Moreover, as shown in Fig. 8(a), the peak of the temperature dependence of ΔS_M broadens with a decrease in particle size. This is because of the gentle decrease in magnetization close to the FM-PM transition of the continuous second-order phase transitions. The details will be discussed later.

For a first-order transition, there is a singularity close to T_C mentioned above and the discontinuous magnetic entropy change around the transition should be taken into account. The $\Delta S_M^{\max}$ of the 43 nm sample for the field changes 0.5, 1.0, 2.0, 3.0, and 4.5 T are about 2.30, 4.73, 6.41, 7.46, and 8.63 J/kgK, respectively. With decreasing particle size the $\Delta S_M^{\max}$ decreases due to the change of phase transition from first order to second order transition as discussed in details later in this article.

The magnetic cooling efficiency of a magnetocaloric material can be evaluated by considering the magnitude of $|\Delta S_M|$ and its full-width of half maximum (δT_{FWHM}).[9] The so-called relative cooling power (RCP) can be expressed as product of $\Delta S_M^{\max}$ and the δT_{FWHM}

$$RCP = |\Delta S_M^{\max}| \times \delta T_{FWHM}. \quad (6)$$

Figure 8(d) shows the H dependence of RCP of 17, 28, and 43 nm samples. It is found that the maximum RCP value of 350 kJ/kg is obtained in the 28 nm sample with $\Delta H = 4.5$ T. This RCP value is much larger than the 17 and 43 nm samples because it has the relatively large $\Delta S_M^{\max}$ as well as broad δT_{FWHM}. The result indicates that the RCP can be maximized by adjusting the particle to a suitable size.

For 17 and 28 nm particles as discussed above $M(H) = M_{core} + M_{shell}$, so we can write Eq. (5) as

$$\begin{aligned}\Delta S_M &= \Delta S_{core} + \Delta S_{shell} \\ &= n_1 \int_{H_1}^{H_2} \left(\frac{\partial M_{core}}{\partial T}\right)_H dH + n_2 \int_{H_1}^{H_2} \left(\frac{\partial M_{shell}}{\partial T}\right)_H dH \\ &= N\mu_s n_1 \int_{H_1}^{H_2} \left(\frac{\partial L(\alpha)}{\partial T}\right)_H dH + \chi n_2 \int_{H_1}^{H_2} \left(\frac{\partial H}{\partial T}\right)_H dH,\end{aligned} \quad (7)$$

where n_1 and n_2 are the content ratio of core and surface and N is the number of particles. The ΔS_M of single domain particles (the 17 and 28 nm samples) is composed by two parts:

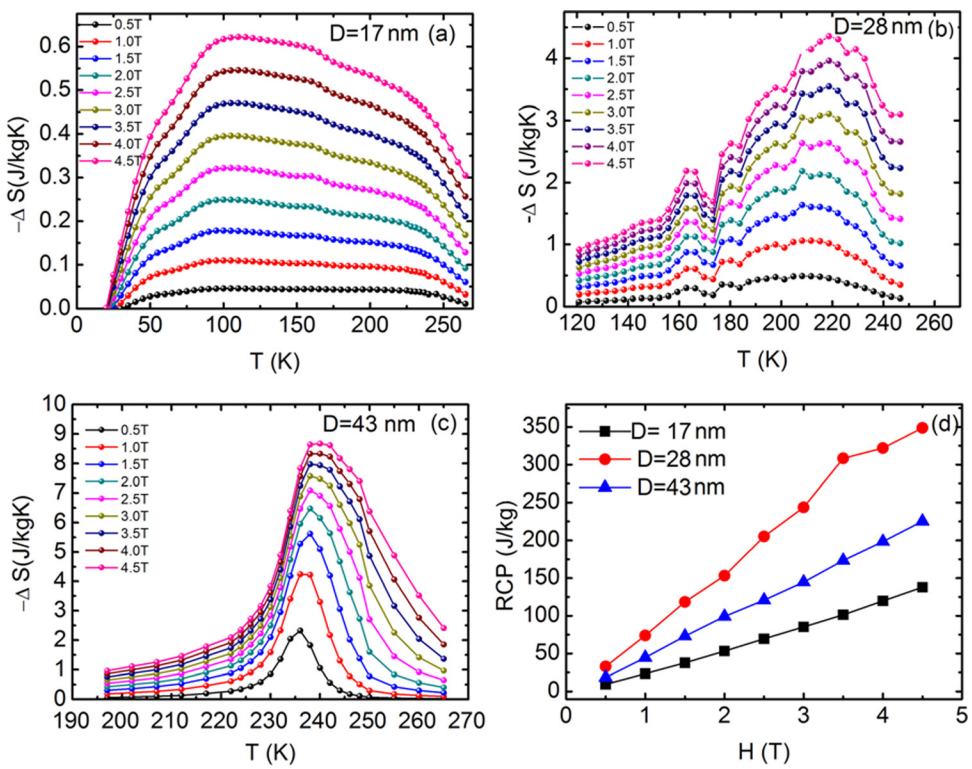

FIG. 8. (a)-(c) Temperature dependence of magnetic entropy change under different magnetic field changes of 0.5–4.5 T; (d) Field dependence of RCP for the selected 17, 28, and 43 nm samples.

the superparamagnetic core induced term (for example, in 17 nm sample it is superparamagnetic at any temperature if the applied field is larger than 0.29 T, since for the field larger than 0.29 T the blocking of SPM and freezing of super-spin-glass both disappear as the fitting data of AT line shows) and disordered surface induced term. $L(\alpha) = coth(\frac{\mu_s H}{kT}) - 1/(\frac{\mu_s H}{kT})$ is the Langevin function, and μ_s is the moment of a single particle. As expected from Eq. (7) the derivative of $L(\alpha)$ is dependent on μ_s which can be decided by spontaneous magnetization (small M_s and gentle change of M_s both induce low ΔS_M but induce broad δT_{FWHM} as expected from Eq. (7)).

For the magnetic core the M_s becomes lower and the change of M_s with T becomes gentle with the decreased particle size (the PM-FM phase transition is changed from first order to second order as particle size decreases), thus low ΔS_M and broad δT_{FWHM} can be induced. On the other hand the shell is nonmagnetic therefore as the particle size decreases the number of the surface atoms increases and the number of the core atoms decreases. Thus the M_s of the core decreases and induced low ΔS_M and broad δT_{FWHM} with decrease in particle size. Meanwhile magnetization of the shell is less dependent on T (the M (H) curves at different temperatures are nearly parallel to each other as shown in Fig. 6 indicating the magnetization of the shell is nearly independent on T), thus the shell induced ΔS_M is small and have a very broad peak. According to the discussions above the entropy change ΔS_M decreases but the peak of the temperature dependence of ΔS_M broadens with a decrease in particle size. Therefore the maximum of RCP can be obtained in a particle system with intermediate size.

The magnetic core follows the Langevin-like function as discussed above. Therefore the entropy change of the core can be expressed as

$$\begin{aligned}\Delta S_M &= N\mu_s \int_{H_1}^{H_2} \left(\frac{\partial L(\alpha)}{\partial T}\right)_H dH \\ &= N\mu_s \int_{H_1}^{H_2} \left(\frac{\partial[\coth(\alpha) - 1/\alpha]}{\partial T}\right)_H dH \\ &= \left[\frac{N{\mu_s}^2}{kT^2} H \operatorname{csc}\mathrm{h}^2\alpha + \frac{N\mu_s}{T}\coth\alpha + \frac{k}{\mu_s}\ln H\right]_{H_1}^{H_2}.\end{aligned} \tag{8}$$

Letting $H_1 = 0$ and $H_2 = \Delta H$,

$$\Delta S_M = N{\mu_s}^2 \Delta H \operatorname{csc}\mathrm{h}^2 \frac{\mu_s \Delta H}{kT} + \frac{N\mu_s}{T}\coth\frac{\mu_s \Delta H}{kT} + \frac{k}{\mu_s} ln(\Delta H). \tag{9}$$

For the large particles (43 nm, for example), the PM-FM transition is of first order, the cores are not superparamagnetic as the particle size is larger than the critical single domain value and the atoms at surface can be ignored compared with atoms in core. The sample behaves like bulk materials and has a large and abrupt variation of ΔS_M, therefore the peak of ΔS_M is narrow, which induces lower RCP.

IV. CONCLUSIONS

In summary, the magnetic properties have been investigated for $La_{0.8}Ca_{0.2}MnO_3$ nanoparticles with average particle size from 17 nm to 43 nm. The results show the existence of superparamagnetism, super-spin-glass, and surface-spin-glass in fine particles. The existence of these states depends on the applied magnetic field. The core-shell structure model is suitable for explaining the magnetic behavior of $La_{0.8}Ca_{0.2}MnO_3$ nanoparticles: The ferromagnetic cores are surrounded by nonmagnetic surface shells. It is found that the transition from paramagnetism to ferromagnetism has been changed from first order to second order as particle size reduced. The temperature dependence of magnetization has been greatly changed with decreasing particle size due to the change of intrinsic magnetization of the inner core. Therefore the magnetocaloric effect was greatly changed by the particle size. The relative cooling power can be tuned dramatically by particle size due to the changed ratio of the shell and surface, the change of spontaneous magnetization and the superparamagnetic behavior of the core. The results indicate that the optimized relative cooling power can be obtained as the particle is of a suitable size.

ACKNOWLEDGMENTS

This work was supported by the National Key Basic Research under Contract No. 2011CBA00111, and the National Nature Science Foundation of China under Contract Nos. 10804111 and 10974205, and Director's Fund of Hefei Institutes of Physical Science, Chinese Academy of Sciences.

[1] R. von Helmolt, J. Wecker, B. Holzapfel, L. Schultz, and K. Sanwer, Phys. Rev. Lett. **71**, 2331 (1993).
[2] S. Jin, T. H. Tiefel, M. McCormack, R. A. Fastnacht, R. Ramesh, and L. H. Chen, Science **264**, 413 (1994).
[3] C. S. Hong, W. S. Kim, and N. H. Hur, Phys. Rev. B **63**, 092504 (2001).
[4] C. P. Adams, J. W. Lynn, V. N. Smolyaninova, A. Biswas, R. L. Greene, W. Ratcliff, I. I. S. W. Cheong, Y. M. Mukovskii, and D. A. Shulyatev, Phys. Rev. B **70**, 134414 (2004).
[5] J. Mira, J. Rivas, F. Rivadulla, C. Vázquez- Vázquez, and M. A. López-Quintela, Phys. Rev. B **60**, 2998 (1999).
[6] V. K. Pecharsky, K. A. Gschneidner, and A. O. Tsokol, Rep. Prog. Phys. **68**, 1479 (2005).
[7] E. Bruck, J. Phys. D. Appl. Phys. **38**, R381(2005).
[8] V. Provenzano, A. J. Shapiro, and R. D. Shull, Nature **429**, 853 (2004).
[9] M. H. Phan and S. C. Yu, J. Magn. Magn. Mater. **308**, 325 (2007).
[10] Z. B. Guo, Y. W. Du, J. S. Zhu, H. Huang, W. P. Ding, and D. Feng, Phys. Rev. Lett. **78**, 1142 (1997).
[11] L. E. Hueso, P. Sande, D. R. Miguéns, and J. Rivasa, J. Appl. Phys. **91**, 1215 (2002).
[12] A. Rostamnejadi, M. Venkatesan, J. Alaria, M. Boese, P. Kameli, H. Salamati, and J. M. D. Coey, J. Appl. Phys. **110**, 043905 (2011).
[13] W. Tang, W. J. Lu, X. Luo, B. S. Wang, X. B. Zhu, W. H. Song, Z. R. Yang, and Y. P. Sun, J. Magn. Magn. Mater. **322**, 2360 (2010).
[14] S. E. Lofland, V. Ray, P. H. Kim, S. M. Bhagat, M. A. Mannheimer, and S. D. Tyagi, Phys. Rev. B **55**, 2749 (1997).
[15] A. K. Pramanik and A. Banerjee, Phys. Rev. B **82**, 094402 (2010).
[16] T. Jonsson, J. Mattsson, C. Djurberg, F. A. Khan, P. Nordblad, and P. Svedlindh, Phys. Rev. Lett. **75**, 4138 (1995).
[17] P. Dey, T. K. Nath, P. K. Manna, and S. M. Yusuf, J. Appl. Phys. **104**, 103907 (2008).
[18] R. C. O'Handley, *Modern Magnetic Materials Principles and Applications* (Wiley-VCH, Weinheim, 2000).
[19] L. Néel, Ann. Geophys. **5**, 99 (1949).
[20] W. F. Brown, Jr., Phys. Rev. **130**, 1677 (1963).
[21] D. S. Fisher and D. A. Huse, Phys. Rev. Lett. **56**, 1601 (1986).
[22] D. S. Fisher and D. A. Huse, Phys. Rev. B **38**, 373(1988).
[23] C. R. Vestal and Z. J. Chang, J. Am. Chem. Soc. **125**, 9828 (2003).
[24] D. A. Garanin and H. Kachkachi, Phys. Rev. Lett. **90**, 065504 (2003).
[25] L. Almeida, Jr. and D. J. Thouless. J. Phys. A **11**, 983 (1978).
[26] M. E. Hilo, K. O. Grady, and R. W Chantrell, J. Magn. Magn. Mater. **114**, 307 (1992).
[27] H. Mamiya and I. Nakatani, J. Magn. Magn. Mater. **177**, 966 (1998).

[28]B. Martínez, X. Obradors, L. Balcells, A. Rouanet, and C. Monty, Phys. Rev. Lett. **80**, 181 (1998).
[29]V. Spasojevic, A. Mrakovic, M. Perovic V. Kusigerski, and J. Blanusa, J. Nanopart. Res. **13**, 763 (2011).
[30]M. Garcíadel Muro, X. Batlle, and A. Labarta, Phys. Rev. B **59**, 13584 (1999).
[31]S. A. Majestich and M. Sachan, J. Phys. D Appl. Phys. **39**, R407 (2006).
[32]S. Morup, Europhys. Lett. **28**, 671 (1994).
[33]R. D. Zysler, C. A. Ramos, E. De Biasi, H. Romero, A. Ortega, and D. Fiorani, J. Magn. Magn. Mater. **221**, 1 (2000).
[34]S. Bedanta and W. Kleemannl J. Phys. D Appl. Phys. **420**, 13001 (2009).
[35]V. Markovich, I. Fita, A. Wisniewski, G. Jung, D. Mogilyansky, R. Puzniak, L. Titelman, and G. Gorodetsky, Phys. Rev. B **81**, 134440 (2010).
[36]T. Zhu, B. G. Shen, J. R. Sun, H. W. Zhao, and W. S. Zhan, Appl. Phys. Lett. **78**, 3863 (2001).
[37]E. Rozenberg, M. Auslender, A. I. Shames, G. Jung, I. Felner, M. I. Tsindlekht, D. Mogilyansky, E. Sominski, A. Gedanken, Y. M. Mukovskii, and G. Gorodetsky, J. Appl. Phys. **110**, 073919 (2011).
[38]L. Zheng, K. B. Li, and Y. H. Zhang, Phys. Rev. B **58**, 8613 (1998).
[39]E. De Biasi, C. A. Ramos, and R. D. Zysler, Phys. Rev. B **65**, 144416 (2002).
[40]S. K. Banerjee, Phys. Lett. **12**, 16 (1964).
[41]D. Balzar and H. Ledbetter, J. Appl. Crystallogr. **26**, 97 (1993).
[42]R. H. Kodama, J. Magn. Magn. Mater. **200**, 359 (1999).
[43]T. Hashimoto, T. Numasawa, M. Shino, and T. Okada, Cryogenics **21**, 647 (1981).
[44]V. K. Pecharsky and K. A. Gschneidner, Jr., J. Appl. Phys. **86**, 565 (1999).
[45]V. K. Pecharsky, K. A. Gschneidner, Jr., A. O. Pecharsky, and A. M. Tishin, Phys. Rev. B **64**, 44406 (2001).